Transition Met Chem
DOI 10.1007/s11243-016-0062-3

Ruthenium complexes with lumazine derivatives: structural, electrochemical, computational and radical scavenging studies

Abimbola Adebisi[1] · Irvin Noel Booysen[1] · Matthew Piers Akerman[1] · Bheki Xulu[1]

Received: 4 April 2016 / Accepted: 12 May 2016

Abstract In this research study, the formation and characterization of new ruthenium(II) and (III) complexes encompassing multidentate ligands derived from 6-acetyl-1,3,7-trimethyllumazine (almz) are reported. The 1:1 molar coordination reactions of *trans*-[$RuCl_2(PPh_3)_3$] with *N*-1-[1,3,7-trimethyllumazine]benzohydride (bzlmz) and 6-(*N*-methyloxime)-1,3,7-trimethyllumazine (ohlmz) formed a diamagnetic ruthenium(II) complex, *cis*-[$RuCl_2$(bzlmz)(PPh_3)] (**1**), and paramagnetic complex, *cis*-[$Ru^{III}Cl_2$(olmz)(PPh_3)] (**2**) [Holmz = 6-(*N*-hydroxy-*N*′-methylamino)-1,3,7-trimethyllumazine], respectively. These ruthenium complexes were characterized via physico-chemical and spectroscopic methods. Structural elucidations of the metal complexes were confirmed using single crystal X-ray analysis. The redox properties of the metal complexes were investigated via cyclic voltammetry. Electron spin resonance spectroscopy confirmed the presence of a paramagnetic metal centre in **2**. The radical scavenging activities of the metal complexes were explored towards the DPPH and NO radicals. Quantum calculations at the density functional theory level provided insight into the interpretation of the IR and UV–Vis experimental spectra of **1**.

Electronic supplementary material The online version of this article (doi:10.1007/s11243-016-0062-3) contains supplementary material, which is available to authorized users.

✉ Irvin Noel Booysen
Booyseni@ukzn.ac.za

[1] School of Chemistry and Physics, University of KwaZulu-Natal, Private Bag X01, Scottsville, Pietermaritzburg 3209, South Africa

Introduction

The exploration of ruthenium in medicinal inorganic chemistry is largely due to the discovery of NAMI A, *trans*-[$RuCl_4$(DMSO)(Im)](ImH) {ImH = protonated imidazole} and KP1019 (*trans*-tetrachlorobis(indazole)ruthenate(III)) as potential metal-based anticancer drugs [1, 2]. Their high cytotoxicity towards metastatic tumours is accounted to the fact that ruthenium is a group congener of the essential element, iron, and these first-generation ruthenium chemotherapeutic drugs share similar biodistribution patterns as iron [3, 4]. However, more innovative drug design strategies are required to negate the common side effects associated with chemotherapy [5].

A current design strategy entails the use of scaffolds encompassing biologically significant moieties within the coordination sphere of ruthenium complexes [6]. These biologically significant moieties may promote the physiological biocompatibility of the ruthenium complex and can also facilitate a target-specific biodistribution towards tumours [7]. Hence, the design of new target-specific ruthenium chemotherapeutic drugs provides scope for exploring the fundamental coordination chemistry of ruthenium towards biologically relevant ligand systems.

A plausible candidate as a biologically active moiety is lumazine which is a derivative of the enzyme, Lumazine synthase [8]. Lumazine synthase plays a pivotal role in the body through catalysing the formation of riboflavin (vitamin B2) [9]. Deficiency of riboflavin has been found to be associated with high tendencies of breast and cervical cancer occurrences [10]. Moreover, one of the annealed ring systems of lumazine is a uracil which is a constituent of well-established chemotherapeutic drugs, uramustine and 5-fluoro-uracil [11]. In fact, the coordination susceptibility of Schiff bases derived from 5, 6-diamino-1,

Published online: 20 May 2016

3-dimethyluracil towards ruthenium has been demonstrated [12, 13].

Herein, the isolation of new ruthenium complexes containing ligands derived from 6-acetyl-1,3,7-trimethyllumazine (almz) is reported. The coordination reactions using *trans*-[$RuCl_2(PPh_3)_3$] as the metal precursor yielded the diamagnetic ruthenium(II) complex, *cis*-[$RuCl_2$(bzlmz)(PPh_3)] (**1**), and paramagnetic ruthenium(III) complex, *cis*-[$RuCl_2$(olmz)(PPh_3)] (**2**). The resultant metal complexes were spectroscopically characterized and structurally elucidated with single-crystal X-ray analysis. In addition, the potential antioxidant capabilities of these metal complexes were evaluated by means of radical scavenging studies with DPPH and NO radicals.

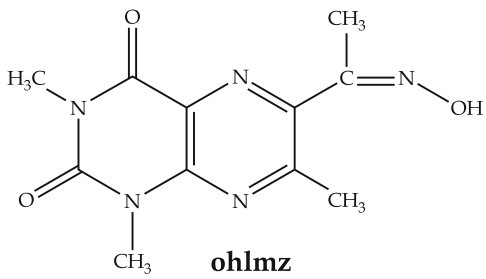

ohlmz

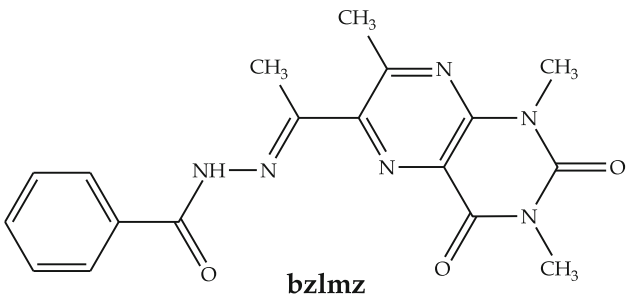

bzlmz

Experimental

Materials and methods

Trans-[$RuCl_2(PPh_3)_3$], 6-amino-1,3-dimethyl-5-nitrosouracil, acetylacetone, benzhydrazide, hydroxylamine hydrochloride, 2,2-di(4-*tert*-octylphenyl)-1-picrylhydrazyl (DPPH), Griess reagent, sodium nitroprusside, phosphate-buffered saline (PBS) tablets and electrochemical-analysis-grade tetrabutylammonium hexafluorophosphate were obtained from Sigma-Aldrich. All solvents and common salts were obtained from Merck SA. Reagent-grade toluene was dried over sodium wire while the other solvents and the other chemicals were used without any further purification. Ultrapure water was produced from an Elga Purelab Ultra system. The pro-ligand, 6-acetyl-1,3,7-trimethyllumazine (almz) was obtained from the reaction of 6-amino-1,3-dimethyl-5-nitrosouracil with acetylacetone [14]. The synthetic procedures and characterization data for the free ligands (viz. bzlmz and ohlmz) can be found in the online supporting information document (figures S1–S4). The synthetic procedure for bzlmz was adopted and modified from a method previously reported [15]. The free ligand, ohlmz, was isolated from an experimental procedure attained from the literature [16].

The infrared spectra were recorded on a PerkinElmer Spectrum 100 in the 4000–350 cm^{-1} range. The ^1H nuclear magnetic resonance and ^{31}P spectra were obtained using a Bruker Avance 400 MHz spectrometer. All NMR spectra were recorded in deuterated dimethylsulphoxide. UV–Vis spectra were recorded using a PerkinElmer Lambda 25. The extinction coefficients (ε) are given in $dm^3\ mol^{-1}\ cm^{-1}$. Melting points were determined using a Stuart SMP3 melting point apparatus. The conductivity measurements were determined at 295 K on a Radiometer R21M127 CDM 230 conductivity and pH meter. Elemental analysis (EA) was carried out using a CHNS-O Flash 2000 Organic Elemental Analyser. Mass spectrometry (MS) was conducted in both the positive and negative modes via direct injection of the samples into a Waters Micromass LCT Premier MS instrument equipped with an electrospray ionization (ESI) source and a time-of-flight (TOF) mass analyser.

Voltammetric measurements were done using an Autolab potentiostat equipped with a three electrode system: a glassy carbon working electrode (GCWE), a pseudo Ag|AgCl reference electrode and an auxiliary Pt counter electrode. The Autolab Nova 1.7 software was utilized for the operation of the potentiostat and data analysis. The ruthenium metal complexes were made up in 2 mM solutions in CH_2Cl_2 along with tetrabutylammonium hexafluorophosphate (0.1 M) as a supporting electrolyte. Between each measurement, the GCWE electrode surface was polished with a slurry of ultrapure water and alumina on a Buehler felt pad followed by rinsing with excess ultrapure water as well as ultra-sonication in absolute ethanol.

The experimental procedures of the radical scavenging studies were adapted from the literature methods [17, 18]. All experiments were run in triplicate, and the percentage radical scavenging activities were determined via the following equation:

$$\%\text{Radical scavenging activity} = [(A_c - A_f)/A_c] \times 100$$

where A_c is the absorbance of the control (DPPH or NO radicals) and A_f is the absorbance upon addition of the ligand or metallic compound to the control. In turn, the IC_{50} values of the respective ligands and their metallic compounds were calculated from the percentage radical scavenging activity. Each IC_{50} value has a standard deviation less than 3 % with respect to its mean value. Firstly,

the UV–Vis spectrum of the control [0.2 mM solution of DPPH in dichloromethane (DCM)] was measured, and thereafter 0.1 cm^3 of the metallic compound or the free ligand (30 μM in DCM) was added. The resultant solutions were shaken vigorously and left to stand for 20 min in the dark, and then their respective UV–Vis spectra were measured. The vitamin C analysis was done in a similar manner with the exception that both the vitamin C solution and its DPPH control solution were prepared in methanol.

The NO radical assay was done using the following experimental procedure: a 5 mM solution of sodium nitroprusside was prepared in phosphate-buffered saline solution. The Griess reagent (0.5 cm^3) was added to 0.3 cm^3 of the nitroprusside solution. The UV–Vis spectrum of the mixture was taken which constitutes the control. The sample solutions were prepared by adding 1 cm^3 of the metal complex, vitamin C or the free ligand (30 μM in DMSO) to a 0.3 cm^3 volume of sodium nitroprusside solution, and the resultant mixture was allowed to incubate for 3 h at room temperature. After the incubation period, 0.5 cm^3 of the Griess reagent was added, which was followed by measurement of the respective UV–Vis spectra.

Preparation of cis-[$RuCl_2$(bzlmz)(PPh_3)] (1)

A mixture of bzlmz (0.04 g; 0.10 mmol) and *trans*-[$RuCl_2(PPh_3)_3$] (0.10 g; 0.10 mmol) was dissolved in 20 ml of toluene. The resultant solution was heated until reflux for 6 h and filtered. Slow evaporation of the mother liquor gave dark brown crystals suitable for X-ray analysis. Yield = 0.06 g (68 %); M.P = 280–282 °C; IR (ν_{max}/cm^{-1}): ν(N–H)$_{amide}$ 3374 (w), υ(C=O)$_{lumazine}$ 1710, 1692 (s), υ(C=O)$_{amide}$ 1623 (s), υ(C=N)$_{lumazine}$ 1534 (s), ν(C–N)$_{amide}$ 1268 (m), ν(Ru-PPh_3) 695 (vs); ^{1}H NMR (295 K/ppm): 11.0 (s, 1H, *N6*), 9.36 (s, *toluene*), 8.2 (d, 2H, *H14*, *H18*), 7.7–7.1 (m, 18H, *H15*, *H16*, *H17*, *PPh$_3$*), 3.6 (s, 3H, *C8–H$_3$*), 2.7 (d, 6H, *N1–CH$_3$, N2–CH$_3$*), 2.1 (s, 3H, *C11–H$_3$*); ^{31}P NMR (295 K/ppm): 25.6; UV–Vis (DCM, [λ_{max} (ε, M^{-1} cm^{-1})]): 300 nm (19139), 366 nm (10931), 447 nm (7392), 677 nm (474); Conductivity (DCM, 10^{-3} M): 9.2 O^{-1} cm^{-2} mol^{-1}; Anal. Calc. for $C_{43}H_{40}Cl_2N_6O_3PRu$ (%): C, 57.9; H, 4.5; N, 9.4. Found: C, 58.0; H, 4.2; N, 9.0; TOF–MS (*m/z*): Calcd: 909.1 [M]; Found: 799.1 [M-H_2O–C_7H_8].

Preparation of *cis*-[$RuCl_2$(olmz)(PPh_3)] (2)

The title compound was formed from the 1:1 molar ratio reaction of ohlmz (0.03 g; 0.10 mmol) with *trans*-[$RuCl_2(PPh_3)_3$] (0.10 g, 0.10 mmol) in 20 ml of toluene after 6 h of heating at reflux temperature. A maroon precipitate was filtered off and recrystallized by the slow diffusion of dichloromethane into *n*-hexane [1:1 (*v:v*)], which resulted in the formation of brown XRD quality crystals. Yield = 0.04 g (63 %); M.P > 350 °C; IR (ν_{max}/cm^{-1}): ν(C=O) 1688, 1620 (vs), ν(C=N) 1559 (m), ν(Ru–PPh_3) 696 (s); UV–Vis (DCM, [λ_{max} (ε, M^{-1} cm^{-1})]): 350 nm (6502), 461 nm (6646), 707 nm (550); Conductivity (DCM, 10^{-3} M): 15.0 O^{-1} cm^{-2} mol^{-1}; Anal. Calc. for $C_{28}H_{27}Cl_2N_5O_3PRu$ (%): C, 49.1; H, 4.0; N, 10.2. Found: C, 49.1; H, 4.0; N, 9.9; TOF–MS (*m/z*): Calcd: 684.0 [M]; Found: 684.0 [M].

X-ray diffraction

The X-ray data for the metal complexes were recorded on a Bruker Apex Duo equipped with an Oxford Instruments Cryojet and an Incoatec microsource operating at 30 W power. Crystal and structure refinement data for **1** are given in Table 1. The bond lengths and angles for **1** are given in Table 2 for **1**. C_7H_8·H_2O. Only a low-resolution structure could be obtained for **2** (figure S3). In both cases, the data were collected with Mo Kα (λ = 0.71073 Å) radiation at a crystal-to-detector distance of 50 mm. The following conditions were used for data collection: omega and phi scans with exposures taken at 30 W X-ray power and 0.50°

Table 1 Crystal data and structure refinement data

	1 H_2O·C_7H_8
Chemical formula	$C_{43}H_{43}Cl_2N_6O_4PRu$
Formula weight	910.77
Temperature (K)	100(2)
Crystal system	Triclinic
Space group	$P-1$
Unit cell dimensions (Å, °)	a = 10.162(5)
	b = 13.587(5)
	c = 16.268(5)
	α = 105.202(5)
	β = 106.096(5)
	γ = 103.762(5)
Crystal size (mm)	0.19 × 0.18 × 0.12 mm
V (Å^3)	1962.2 (13)
Z	2
Density (calc.) (Mg/m^3)	1.541
Absorption coefficient (mm^{-1})	0.629
F(000)	936
θ range for data collection (°)	1.39; 26.05
Reflections measured	31830
Observed reflections [$I > 2\sigma(I)$]	7117
Independent reflections	7653
Data/restraints/parameters	7653/1/527
Goodness of fit on F^2	1.078
Observed R, wR^2	0.0336; 0.0824
R_{int}	0.026

Table 2 Selected bond lengths [Å] and bond angles [°] for **1**

	Experimental	Optimized
Ru–P	2.333(8)	2.4066
Ru–N4	1.903(2)	1.9525
Ru–N5	2.003(3)	2.0056
Ru–Cl1	2.412(1)	2.4821
Ru–Cl2	2.4527(9)	2.4481
C12–O3	1.222(3)	1.2175
C2–O1	1.248(4)	1.2357
C4–O2	1.210(4)	1.2109
N5–Ru–N4	77.47(9)	78.291
N4–Ru–O1	78.47(8)	78.887
N5–Ru–O1	155.84(8)	153.174
Cl1–Ru–N4	173.42(7)	171.196

frame widths using APEX2 [19]. The data were reduced with the program SAINT [19] using outlier rejection, scan speed scaling, as well as standard Lorentz and polarization correction factors. A SADABS semi-empirical multi-scan absorption correction [20] was applied to the data. Direct methods, SHELX-2014 [21] and WinGX [22] were used to solve both structures. All non-hydrogen atoms were located in the difference density map and refined anisotropically with SHELX-2014 [21]. All hydrogen atoms were included as idealised contributors in the least squares process. Their positions were calculated using a standard riding model with C–$H_{aromatic}$ distances of 0.93 Å and $U_{iso} = 1.2\ U_{eq}$, C–$H_{methylene}$ distances of 0.99 Å and $U_{iso} = 1.2\ U_{eq}$ and C–H_{methyl} distances of 0.98 Å and $U_{iso} = 1.5\ U_{eq}$. The hydrogen atoms of the water molecule and the amino NH of **1** were located in the difference density map and refined isotropically. The O1w–H2w bond distance was restrained using a DFIX command with a distance of 087 Å and ESD = 0.02. Disordered solvent in the lattice of compound **2** was removed using the Platon SQUEEZE routine [23]. This left solvent accessible voids of 566 $Å^3$.

Computational details

Quantum calculations were conducted with GAUSSIAN 09 W [24]. Geometry optimization of the ruthenium complex **1** was achieved through a DFT calculation using the B3LYP functional, with an accompanying hybrid basis set viz. the 6-311G^{++} (*d, p*) basis set was applied to all the C, H, N, O, Cl and P atoms and the LANL2DZ basis set, which makes use of effective core potentials, applied to the metal centre [25]. Prior to the calculation, the solvent molecules of recrystallization for **1** were omitted from the crystal structure, and the resultant structure was used as the starting conformer. Good agreement was found between the optimized and geometrical parameters (refer to Table 2) with the minor deviations attributed to the fact that gas-phase-optimized structures do not account for non-classical hydrogen bonding interactions or any short distance contacts. Using the optimized structure of the metal complex, the lack of any negative eigenvalues in the frequency calculations confirmed that the structure is at a global minimum on the potential energy surface [26].

Results and discussion

Synthesis, spectral characterization and computational studies

The ruthenium(II) and (III) complexes **1** and **2** were formulated from the 1:1 molar coordination reactions between *trans*-[$RuCl_2(PPh_3)_3$] and their respective free ligands, bzlmz and ohlmz, respectively. In **1** and **2**, the bzlmz and olmz chelators coordinate via their respective tridentate $N_{imino}N_{pyrazine}O_{ketonic}$ and $O_{ketonic}N_{pyrazine}O_{nitroso}$ donor sets (Figs. 1 and S3). Interestingly, a fascinating transformation is observed from the free ligand, ohlmz to the olmz chelator, refer scheme S1.

The IR spectra of bzlmz and its complex (figure S4) show numerous vibrations between 1200 and 1800 cm^{-1} which are poorly resolved due to the extended π-conjugation within bzlmz. However, frequency calculations aided in the interpretation of these vibrations (figure S5). More specifically, the simulated spectrum of **1** indicated a distinctive difference between coordinated and uncoordinated ketonic vibrations at 1669 and 1776 cm^{-1}, respectively. In the overlay IR spectra of **1** and its free ligand, the lumazine ketonic stretches appear as an intense broad vibrational band at 1694 cm^{-1} (for the free ligand, bzlmz), which splits into two vibrational bands at 1692 cm^{-1} (coordinated) and 1710 cm^{-1} (uncoordinated) in **1**.

The $\nu(C{=}O)_{amide}$ is observed at 1740 cm^{-1} in the simulated spectrum of **1** while in the experimental spectra of **1** and its free ligand, the amide C=O vibrations [1623 cm^{-1} for **1** and 1652 cm^{-1} for bzlmz free ligand] are found below the ketonic lumazine vibrations. The simulated amide C–N (1265 cm^{-1}) and C=N (1561 cm^{-1}) stretches compare well with the corresponding wavenumbers found for the peak in the experimental spectra of **1** [ν(C=N) at 1534 cm^{-1} and ν(C–N) at 1268 cm^{-1}] and its free ligand [ν(C=N) at 1547 cm^{-1} and ν(C–N) at 1268 cm^{-1}]. For **1**, the N–H bond vibrates essentially at the same positions at 3374 and 3377 cm^{-1} in the experimental and simulated IR spectra, respectively. In both the experimental IR spectra of **1** and **2**, an intense characteristic ruthenium to triphenylphosphine signal is observed as 695 and 696 cm^{-1}, respectively (figure S6) [27].

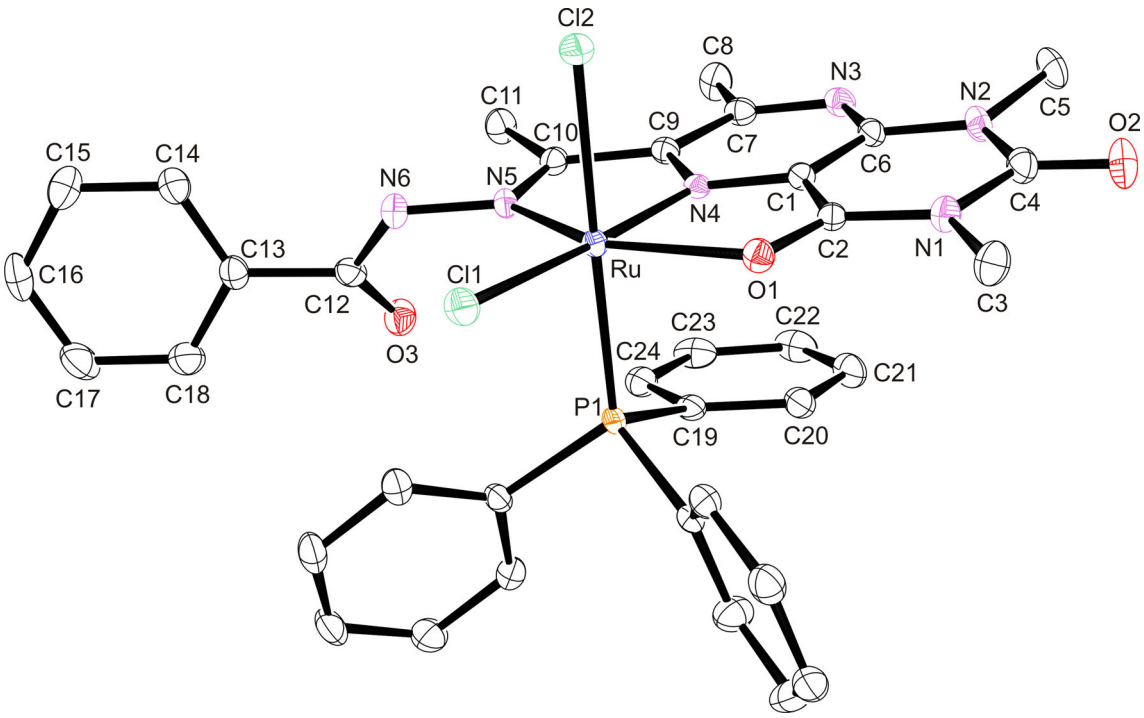

Fig. 1 An ORTEP view of compound **1** showing 50 % probability displacement ellipsoids and the atom labelling. The hydrogen atoms and toluene molecule of crystallization were omitted for clarity

The ^{1}H NMR spectrum of **1** is dominated by an intense multiplet attributed to the signals of the triphenylphosphine co-ligand and selected phenylic protons of the bzlmz chelator (figure S7). The remaining aromatic signal resonates as a doublet at 8.2 ppm. The amide and methyl signals of the bzlmz chelator in **1** are found essentially at the same positions to analogous signals found within the proton spectrum of the corresponding free ligand, bzlmz. As expected, only one signal is observed in the ^{31}P NMR spectrum of **1** for its triphenylphosphine co-ligand (figure S8).

The UV–Vis spectra of the metal complexes both show intense π–π* intraligand transitions below 400 nm associated with the conjugated bzlmz (in **1**) and olmz (in **2**) chelators (figure S9 and S10). At more redshifted regions (between 400 nm and 600 nm), distinctive charge transfer bands appear; a metal-to ligand charge transfer band at 477 nm and ligand-to-metal charge transfer band at 461 nm for **1** and **2**, respectively. Despite complex **1** having a low-spin d^6 electron configuration, it also has a metal-based *d–d* electronic transition such as observed for the paramagnetic complex **2** [677 nm for **1** and 707 nm for **2**]. The presence of the metal-based electronic transition of **1** is ascribed to a low-band-gap energy (2.685 eV) which makes the *d–d* electronic transition favourable. This finding concurs with our previous report where comparable band gap energies were attained for the optimized structures of the ruthenium(II) complex cation, $[RuCl(Hobz)_2(PPh_3)]^+$ (Hobz = 2-hydroxyphenylbenzimidazole) [band-gap energy = 3.189 eV] and the paramagnetic ruthenium complex, $[Ru^{III}Cl(obs)_2(PPh_3)]$ [band-gap energy = 3.236 eV]; this computational data explained why both these metallic compounds had distinctive *d–d* electronic transitions [28].

The EPR spectrum of **2** (figure S11) was obtained only in the solid-state at room temperature. A low resolution singlet (g value = 2.01) confirmed the presence of the paramagnetic metal centre of complex **2** in the solid-state at 298 K. The nature of the EPR spectrum of **2** is characteristic of some low spin ruthenium(III) octahedral complexes [29]. The EA data compare well with the calculated exact masses of the respective metal complexes while the low resolution mass spectra of **1** and **2** showed peaks corresponding to $[M\text{-}H_2O\text{–}C_7H_8]$ at *m/z* 799.1 and [M] at *m/z* 684.0 (figures S12 and S13).

Electrochemistry studies

The CVs of **1** and **2** showed single redox couples attributed to the Ru(II)/Ru(III) redox couples as seen in figure S14. The assignment is made based on the fact that their half-wave potentials [$E_{½}$ = 0.96 V (for **1**) and 0.83 V (for **2**) vs. Ag|AgCl] reside in the potential window of −0.15 and 0.96 V for halfwave potentials attained for mononuclear diamagnetic and paramagnetic ruthenium complexes under

similar electrochemical conditions [28, 30]. In addition, these redox couples correspond to one-electron redox processes governed by their peak to peak separations (I_{pa}/I_{pc}) approaching 1. Furthermore, the redox couples are quasi-reversible as the peak-to-peak separations of **1** ($\Delta E = 80$ mV) and **2** ($\Delta E = 70$ mV) are smaller than that of the standard ferrocene (90 mV at 100 mV/s), indicating faster electron transfer kinetics for the metal complexes. Also, the two redox couples displayed diffusion-controlled behaviour with increasing scan rates. For instance, figure S15 shows overlay CVs of complex **2** for scan rates ranging from 25 to 200 mV/s, at increments of 25 mV/s.

Radical scavenging studies

The mutation of healthy cells by free radicals is reported to be a common cause of cancer, Alzheimer's disease and cardiovascular diseases [31, 32]. To deter the negative effects of these free radicals, more effective radical scavengers are required other than the natural antioxidant, vitamin C. Previous studies have illustrated that ruthenium compounds can be effective radical scavengers, largely owing to their optimal redox properties [33]. Indicative of these previous studies, the formulated ruthenium compounds **1** and **2** with lumazine moieties are found to have significantly higher DPPH [IC_{50}(DPPH) = 46 μM (for **1**) and 63 μM (for **2**)] and NO [IC_{50}(NO) = 36 μM (for **1**) and 34 μM (for **2**)] radical scavenging activities in comparison with vitamin C [IC_{50}(NO) = 210 μM and IC_{50} (DPPH) = 147 μM] [33–35]. Furthermore, the metallic compounds have lower IC_{50} values than their corresponding ligands [IC_{50}(DPPH) = 392 μM (for bzlmz) and 109 μM (for ohlmz); IC_{50}(NO) = 1002 μM (for bzlmz) and 125 μM (for ohlmz)] which emphasizes the influence of the metal atoms in **1** and **2**.

In fact, the influence of the bzlmz chelator on the radical scavenging capability of **1** can be regarded as negligible. This deduction is based on the high IC_{50} values of the free ligand, bzlmz, when used for the scavenging of the DPPH and NO radicals, respectively. In contrast to metal-centred radical scavenging activity of **1**, the IC_{50} values of the free ligand, ohlmz, suggested that there could be a synergistic mechanistic effect of radical activity induced by the redox activity of the metal centre and the donation of hydrogen by the olmz chelator of **2**.

Crystallographic studies

Complex **1** co-crystallizes with a water and a toluene molecule of recrystallization within its crystal lattice (Fig. 1). Molecules of **1** afford chains parallel to the [a]-axis induced by hydrogen bonding between the water molecule and adjacent molecules of **1** [O4–HB···N3 = 2.15(7) Å and O4–HA···Cl2 = 2.22(5) Å, N6–H44···O4 = 2.02(4) Å] (figure S16). The crystal lattice of **1** is further stabilized by classical pi–pi interactions between the C19–C24 phenyl ring (of the triphenylphosphine co-ligand) and the C7C9N4C1C6N3 ring (of the bzlmz chelator) defined by the centroid-to-centroid distance of 3.370(3) Å. Intermolecular interactions are also observed between the nearly co-planar toluene molecule and C6C1C2N1C4N2 ring (of the bzlmz chelator) with an interplanar spacing of 3.771(3) Å (figure S17). The aforementioned intermolecular interactions induced the molecules of **1** to stack in columns aligned with the [b]-axis.

The constrained five-membered chelate rings within **1** [N5–Ru–N4 = 77.47(9)° and N4–Ru–O1 = 78.47(8)°] afforded severe deviation in its octahedral geometry, revealed by the equatorial angles [N5–Ru–O1 = 155.84(8)°, Cl1–Ru–N4 = 173.42(7)° for **1**] all deviating from linearity. Furthermore, the lumazine moiety of **1** lies significantly out of the plane [by 87.3(2)°] of the C13–C18 phenyl ring which accounts to the flexibility of the amide aliphatic group. The bond order of the C12–O3 [1.222(3) Å] bond of **1** is confirmed based on its similar distance in comparison with the ketonic C=O bonds within **1** [C2–O1 = 1.248(4) Å and C4–O2 = 1.210(4) Å]. The Lewis acidic character of the diamagnetic ruthenium atom (in **1**) affords a shorter Ru–P [2.333(8) Å] than the analogous bond (Ru–P = 2.3437(7) Å) found in the paramagnetic ruthenium complex, [$Ru^{III}Cl(obs)_2(PPh_3)$] [28]. In addition, the difference in the *cis*-oriented Ru–Cl bonds of **1** [Ru–Cl1 = 2.412(1) Å and Ru–Cl2 = 2.4527(9) Å] are accounted to the variable *trans*-influence imposed on the halides. The ruthenium-to-lumazine nitrogen coordination bond length of **1** is 1.903(2) Å.

Although no ruthenium compounds (besides **1**) bearing lumazine moieties can be found in the Cambridge Crystallographic Data Centre (CCDC), several transition metal complexes with lumazine chelates have been isolated [15, 36–40]. Among these transition metal complexes, the lumazine moiety and its multidentate chelators exhibit diverse coordination modes affording metal complexes with unique molecular geometries. In addition, several of these metal complexes exhibit unique anticancer activities while the presence of the lumazine moiety within the coordination sphere of various *d*-block metals induces unique luminescent behaviours [37, 40].

Conclusion

Novel diamagnetic and paramagnetic ruthenium complexes with multidentate lumazine chelates were formed and spectroscopically characterized. Quantum calculations at the DFT level aided in the interpretation of the experimental

spectra of the metal complex **1**. X-ray analysis affirms the structural elucidations, indicating the metal atoms are in the centres of distorted coordination spheres which are induced by their respective constrained equatorial bite angles. The formulated ruthenium compounds **1** and **2** show excellent capabilities for scavenging the DPPH and NO radicals judged by their significant lower IC_{50} values than their corresponding free ligands and reported IC_{50} values of the natural antioxidant, vitamin C.

Supporting information

CCDC 1463919 contains the supplementary crystallographic data for this paper. These data can be obtained free of charge from The Cambridge Crystallographic Data Centre via www.ccdc.cam.ac.uk/data_request/cif. Supplementary figures S1–S17 associated with this article can be found in the online version.

Acknowledgements We are grateful to the University of KwaZulu-Natal and the National Research Foundation of South Africa for financial support. The authors would like to thank the Department of Chemistry at the Nelson Mandela Metropolitan University for the single crystal X-ray analysis of the initial solid-state structure of complex **1**.

References

1. Murray BS, Babak MV, Hartinger CG, Dyson PJ (2016) Coord Chem Rev 306:86–114
2. Mjos KD, Orvig C (2014) Chem Rev 114:4540–4563
3. Aitken JB, Antony S, Weekley CM, Lai B, Spiccia L, Harris HH (2012) Metallomics 4:1051–1056
4. Koiri RK, Mehrotra A, Trigun SK (2013) Med Hypotheses 80:841–846
5. Oprea AD, Russell RR, Russell KS, Abu-Khalaf M (2015) J Cardiothorac Vasc Anaesth. doi:10.1053/j.jvca.2015.06.020
6. David S, Perkins RS, Fronczek FR, Kasiri S, Mandal SS, Srivastava RS (2012) J Inorg Biochem 111:33–39
7. Wang Z, Qian H, Yiu S, Sun J, Zhu G (2014) J Inorg Biochem 131:47–55
8. Fischer M, Bacher A (2008) Arch Biochem Biophys 474:252–265
9. Bacher A, Eberhardt S, Eisenreich W, Fischer M, Herz S, Illarionov B, Kis K, Richter G (2001) Vitam Horm 61:1–49
10. Premkumar VG, Yuvaraj S, Sathish S, Shanthi P, Sachdanandam P (2008) Vascul Pharmacol 48:191–201
11. Khan GS, Shah A, Rehman Z, Barker D (2012) J Photochem Photobiol B 115:105–118
12. Booysen IN, Maikoo S, Akerman MP, Xulu B (2014) Polyhedron 79:250–257
13. Booysen IN, Maikoo S, Akerman MP, Xulu B, Munro O (2013) J Coord Chem 66:3673–3685
14. Kim Y, Kim J, Kang Y (1999) J Korean Chem Soc 43:535–539
15. Jiménez-Pulido SB, Linares-Ordóñez FM, Martínez-Martos JM, Moreno-Carretero MN, Quirós-Olozábal M, Ramírez-Expósito MJ (2008) J Inorg Biochem 102:1677–1683
16. Jiménez-Pulido SB, Hueso-Ureña F, Fernández-Liencres MP, Fernández-Gómez M, Moreno-Carretero MN (2013) Dalton Trans 42:530–541
17. Krishnamoorthy P, Sathyadevi P, Senthilkumar K, Muthiah P, Ramesh R, Dharmaraj N (2011) Inorg Chem Commun 14:1318–1322
18. Ramachandran R, Viswanathamurthi P (2013) Spectrochim Acta A103:53–61
19. Bruker APEX2, SAINT, SADABS. Bruker AXS Inc (2010) Madison, Wisconsin, USA
20. Blessing RH (1995) Acta Cryst A51:33–38
21. Sheldrick GM (2008) Acta Cryst A64:112–122
22. Farrugia LJ (2012) J Appl Cryst 45:849–854
23. Spek AL (2009) Acta Cryst D65:148–155
24. Frisch MJ, Trucks GW, Schlegel HB, Scuseria GE, Robb MA, Cheeseman JR, Scalmani G, Barone V, Mennucci B, Petersson GA, Nakatsuji H, Caricato M, Li X, Hratchian HP, Izmaylov AF, Bloino J, Zheng G, Sonnenberg JL, Hada M, Ehara M, Toyota K, Fukuda R, Hasegawa J, Ishida M, Nakajima T, Honda Y, Kitao O, Nakai H, Vreven T, Montgomery JA Jr, Peralta JE, Ogliaro F, Bearpark M, Heyd JJ, Brothers E, Kudin KN, Staroverov VN, Kobayashi R, Normand J, Raghavachari K, Rendell A, Burant JC, Iyengar SS, Tomasi J, Cossi M, Rega N, Millam JM, Klene M, Knox JE, Cross JB, Bakken V, Adamo C, Jaramillo J, Gomperts R, Stratmann RE, Yazyev O, Austin AJ, Cammi R, Pomelli C, Ochterski JW, Martin RL, Morokuma K, Zakrzewski VG, Voth GA, Salvador P, Dannenberg JJ, Dapprich S, Daniels AD, Farkas Ö, Foresman JB, Ortiz JV, Cioslowski J, Fox DJ (2009) Gaussian 09 (Revision A.01). Gaussian Inc, Wallingford CT
25. Booysen IN, Ismail MB, Akerman MP (2013) J Coord Chem 66:4371–4386
26. Al-Noaimi M, El-Baighouthi MI, Abdel-Rahman OS, Haddad SF (2011) Polyhedron 30:1884–1890
27. Muthu Tamizh M, Mereiter K, Kirchner K, Karvembu R (2012) J Organomet Chem 700:194–201
28. Booysen IN, Maikoo S, Akerman MP, Xulu B (2015) Trans Met Chem 40:397–404
29. Subarkhan MM, Ramesh R (2015) Spectrochim Acta A138:264–270
30. Booysen IN, Adebisi A, Munro OQ, Xulu B (2014) Polyhedron 73:1–11
31. Assayag I, Goldstein S, Samuni A, Berkman N (2015) Free Radic Biol Med 87:148–156
32. Lushchak VI (2014) Chem Biol Interact 224:164–175
33. Booysen IN, Adebisi A, Akerman MP (2015) Inorg Chim Acta 433:13–20
34. Ramachandran R, Viswanathamurthi P (2013) Spectrochim Acta A 103:53–61
35. Anitha P, Chitrapriya N, Jung Jang Y, Viswanathamurthi P (2013) J Photochem Photobiol B 129:17–26
36. Jimenez-Pulido SB, Illan-Cabeza NA, Hueso-Urena F, Moreno-Carretero MN (2013) Polyhedron 50:10–15
37. Picon-Ferrer I, Hueso-Urena F, Illan-Cabeza NA, Jimenez-Pulido SB, Martinez-Martos JM, Ramirez-Exposito MJ, Moreno-Carretero MN (2009) J Inorg Biochem 103:94–100
38. Hueso-Urena F, Jimenez-Pulido SB, Fernandez-Liencres MP, Fernandez-Gomez M, Moreno-Carretero N (2008) Dalton Trans 6461-6466
39. Hueso-Urena F, Jimenez-Pulido SB, Moreno-Carretero MN, Quiros-Olozabal M, Salas-Peregrin JM (1998) Inorg Chim Acta 277:103–110
40. Jimenez-Pulido SB, Linares-Ordonez FM, Martinez-Martos JM, Moreno-Carretero MN, Quiros-Olozabal M (2008) Inorg Chem 47:1096–1106